VOL. 4, NO. 10, October 2014 ISSN 2225-7217
ARPN Journal of Science and Technology

http://www.ejournalofscience.org

Curvature vs. Charge of Seleniom CMV-based IPMC Possessing the Discretely Changeable Material Characteristics

[1] Kota Ikeda, [2] Minoru Sasaki, [3] Hirohisa Tamagawa

[1] Graduate School of Advanced Mathematical Sciences, Meiji University, 4-21-1, Nakano, Nakano-ku, Tokyo 165-8525 Japan
[2,3] Department of Mechanical Engineering, Faculty of Engineering, Gifu University, 1-1 Yanagido, Gifu, Gifu, 501-1193 Japan

[1] ikeda@isc.meiji.ac.jp, [2] sasaki@gifu-u.ac.jp, [3] tmgwhrhs@gifu-u.ac.jp

ABSTRACT

Theoretical prediction of bending behavior of IPMC is an important task for the purpose of achieving a practical IPMC actuator. It has gradually become apparent that the bending of IPMC is dominated by the charge imposed on it. However, our latest study revealed that the dependency of the Selenium CMV-based IPMC bending behavior on the charge was unexpectedly a bit complex. The relationship of curvature of the Selenium CMV-based IPMC vs. the total charge imposed on it formed a certain trajectory with time. It was observed that the trajectory formed a clockwise rotational curve, when the Selenium CMV-based IPMC underwent the rectangular pulsated voltage at the environmental absolute humidity less than 10 gm^{-3}. On the other hand, when the environmental absolute humidity was greater than 10 gm^{-3}, the rotational trajectory was counterclockwise with respect to time. Such unusually a bit complex behavior of curvature vs. charge of Selenium CMV-based IPMC was theoretically analyzed by the use of a circuit model which the authors had previously proposed under the assumption that the material characteristics of Selenium CMV-based IPMC were discretely changeable. The circuit model well explained such unusual and complex behavior. Another physics-based analysis, employing viscoelastic model also successfully explained the clockwise and counterclockwise trajectory formation. It was concluded that such a complex bending behavior was due to the mutually distinctive influences of individual charges induced within the IPMC on the bending induction and due to the change of material characteristics of Selenium CMV-based IPMC.

Keywords: *IPMC, bending, circuit model, viscoelastic model, charge, curvature*

1. INTRODUCTION

Ionic polymer metal composite is an electromechanical material consisting of an ion exchange membrane sandwiched between two thin metal layers [1-11]. It exhibits bending under quite low voltage as low as 1 V. Hence, researchers have intensively studied IPMC for the past two decades for the purpose of fabricating a practical low energy consumption bending mode polymer-based actuator of IPMC.

Widely studied IPMC is the Nafion-based IPMC, and Nafion is an ion exchange membrane consisting of fluorocarbon backbone with functional atomic group $–SO_3H$. Nafion-based IPMC contains hydrated mobile cations of H+. Usually IPMC such as the Nafion-based IPMC is operated in aqueous solution – in the highly hydrated state – [1-3], and it is one of unique property of IPMC for actuator. It has been believed that the electrical induction of Nafion-based IPMC bending is due to the shift of mobile hydrated cations contained in Nafion-based IPMC toward cathode [1-3,5]. The shift of the hydrated mobile cations causes the gradient of swelling ratio of the Nafion-based IPMC in the thickness direction, resulting in its bending in the anode direction. As long as this bending mechanism is valid, any ion exchange membrane must be capable of serving as a component of IPMC. In fact, two of the authors of this paper (M. S. and H. T.) have studied the characteristics of IPMC consisting of another ion exchange membrane called Selenium CMV sandwiched between two thin silver layers for the past 10 years or so [12]. Selenium CMV is an ion exchange membrane manufactured by Asahi Glass Co., Ltd. (Tokyo, Japan), and it consists of polyvinylchloride fabric coated with hydrocarbon-based polymer with functional atomic group of $–SO_3H$. So, the structure of Selenium CMV is quite similar to that of Nafion.

Bending control of hydrated IPMC is almost impossible irrespective of whether Nafion- or Selenium CMV-based. This is one of fundamental problems hobbling the research progress of IPMC for fabricating a practical bending mode IPMC actuator [13]. However, in the recent past, it was established that the Selenium CMV-based IPMC exhibited (electrically) well-controllable bending behavior, when subjected to an electric pulse in the highly dehydrated state (not fully dehydrated state), and the degree of bending was not so small even though not in the fully hydrated state. Our investigations on the Selenium CMV-based IPMC characteristics carried out in the past several years led us to believe that the bending curvature of Selenium CMV-based IPMC was basically proportional to the total charge it underwent within experimental error margin [14]. Therefore, we assumed that the precise control of Selenium CMV-based IPMC bending could be achieved by the precise control of charge imposed on the Selenium CMV-based IPMC. This assumption was actually validated experimentally [15]. However, the authors of this paper further scrutinized the bending behavior and found out that the bending behavior of the highly dehydrated Selenium CMV-based IPMC was more complex than previously assumed. We experimentally observed an unusual and a bit complex bending behavior. It is out of the proportionality between the curvature and total charge. In this paper, we will present the experimentally observed unusual and a bit complex bending behavior of highly dehydrated Selenium

CMV-based IPMC and analyze it using circuit model previously proposed [12]. Although the circuit model was an effective tool for predicting the IPMC bending behavior, our circuit model introduced in the ref. [12] heavily resorts to the technique of multi-parameter curve fitting. Hence, the circuit model analysis was not so a fundamental analysis. Therefore, we carried out further analysis of bending employing the physics-based theory of elasticity.

2. SPECIMEN PREPARATION

Selenium CMV-based IPMC was prepared by plating a Selenium CMV sheet with silver through silver mirror reaction. Exact procedure of plating is described in the ref. [16]. Once the silver plating was done, the resultant Selenium CMV-base IPMC was placed in the vacuum environment with desiccant in the desiccators so as to be highly dehydrated (not fully dehydrated).

3. EXPERIMENT

In various environments of absolute humidity conditions, within the range of 4.5 gm^{-3} to 12 gm^{-3}, the bending curvature of highly (not fully) dehydrated Selenium CMV-based IPMC and of total charge imposed on it, under a rectangular voltage pulse train, were simultaneously measured using the experimental procedure described in the ref. [12]. From this experiment, we found a bit complex bending behavior of highly dehydrated Selenium CMV-based IPMC. The observation is described in the next section and we will show the result of theoretical analysis of the bending.

4. RESULTS AND DISCUSSION

We studied the relationship between the Selenium CMV-based IPMC curvature and total charge imposed on it, since it was previously reported that the charge played a central role of determining induced bending curvature [14, 15, 17-19]. It was found in this work that the curvature vs. charge formed a rotational trajectory with time by following a certain rule: time direction of the rotation of trajectory was clockwise as long as the environmental absolute humidity was less than 10 gm^{-3}, while it was counterclockwise as long as the environmental absolute humidity was greater than 10 gm^{-3}.

In this section, the experimental observation of the rotational direction change of trajectory in accordance with the environmental absolute humidity is shown, and it is theoretically analyzed.

4.1 Experimentally observed Curvature vs. Charge

Prior to carrying out bending tests, the highly dehydrated (not fully dehydrated) Selenium CMV-based IPMC was cut into strips, 20 mm in length × 2 mm in width. Hereafter, the strip of Selenium CMV-based IPMC is referred to as Selenium IPMC. The Selenium IPMC was subjected to a rectangular voltage pulse train shown in Fig. 1, the voltage amplitude = 1.5 V and frequency = 1/60 Hz.

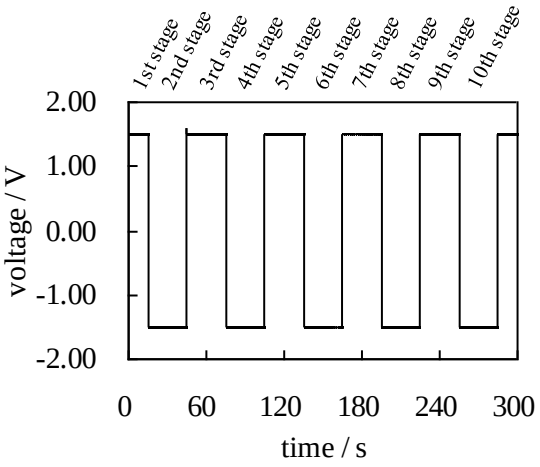

Fig 1: The rectangular, pulsated voltage imposed on the Selenium IPMC vs. time, t 1st stage (0 s < t < 15 s), n the stage (30n - 45 s < t < 30n - 15 s, n = 2, 3, 4 . . .)

Figure 2 shows experimental result of curvature of Selenium IPMC vs. charge imposed on the unit surface area of Selenium IPMC for 105 s at the absolute humidity (AH) = 4.5, 6.8, 10.1 gm^{-3}, where actual measurements were carried out for 300 s. "□" mark in the diagram represents "t = 0 s", and italic number in the diagrams represents the onset moment of individual stage, where the definition of stage is given in Fig. 1. All of these trajectories form a quite long circular curve close to straight line, and this type trajectory have often been observed in the past [14]. Hence, two of the authors of this paper (M. S. and H. T.) initially thought that the trajectory would form a perfect straight line in a quite ideal experimental environment [14]. We carried out the same experiment at various environments of different absolute humidity and observed quite similar trajectories to Fig. 2 repeatedly. During the experiments, we noticed that the trajectory direction was counterclockwise, when the environmental absolute humidity, AH, was beyond 10 gm^{-3}. But as long as AH was lower than 10 gm^{-3}, the clockwise trajectory of curvature vs. charge was observed. In fact, the diagrams of Fig. 2 (a) and (b) were as the result of the experiments carried out at AH < 10 gm^{-3}, and the trajectory directions on both diagrams was clockwise, where clockwise rotation continued even after the onset moment of 5th stage. On the other hand, counterclockwise trajectory of curvature vs. charge was observed, as long as AH was higher than 10 gm^{-3}. Figure 2 (c) was obtained by the experiment carried out at AH > 10 gm^{-3}, and the diagram in it shows counterclockwise trajectory after the onset moment of 3rd stage, where counterclockwise rotation continued even after 5th stage.

To sum up, AH = 10 gm^{-3} is the border at which the trajectory direction changes course with respect to time: clockwise trajectory occurs at AH < 10 gm^{-3}, while the counterclockwise trajectory occurs at AH > 10 gm^{-3}. Straight trajectory was not observed at all, though a number of measurements were taken at around at AH = 10 gm^{-3}.

So, it was speculated that the bending curvature was not perfectly proportional to the charge even at AH = 10 gm^{-3} in the first place. The unidirectional, long circular shaped trajectory rather than the straight trajectory must be inevitably formed even under the quite ideal experimental condition of AH = 10 gm^{-3}. In the following section, the trajectory direction behavior is therefore analyzed using the circuit model previously developed.

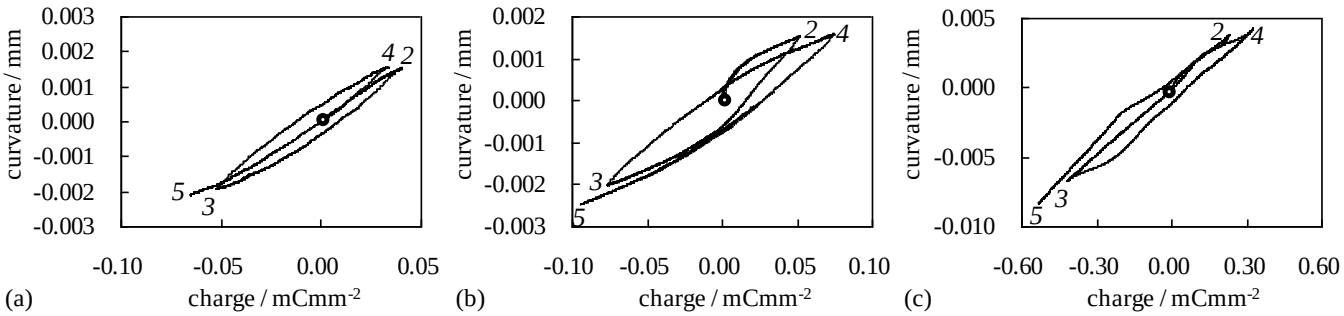

Fig 2: Experimentally obtained trajectory of curvature of Selenium IPMC vs. charge imposed on the unit surface area of Selenium IPMC at (a) AH = 4.5 gm^{-3}, (b) AH = 6.8 gm^{-3} and (c) AH = 10.1 gm^{-3} "O" mark in the diagram represents "t = 0 s". Italic number represents the onset moment of individual stage, where the definition of stage is given in Fig. 1.

4.2 Circuit Model Analysis

Circuit model is often employed for the analysis of IPMC characteristics. For instance, Porfiri derived a circuit model, by which he estimated the charge distribution within IPMC body [17]. His computational result of charge distribution suggests that the ion distribution is significantly altered only at the interface between the electrode and hydrated polymer film layer, and it is quite plausible from the standpoint of electrochemistry. Costa Branco and Dente derived another IPMC circuit model by the electromechanical analysis of IPMC [18]. Structure of their circuit model was a bit different from Porfiri's. As a matter of fact, there are various circuit models of IPMC simplifying actual IPMC systems [17,18,20-22]. The search for the optimal circuit for the analysis of the IPMC characteristics is still ongoing.

Previously we proposed a circuit model for predicting the bending behavior of IPMC which was same as Selenium IPMC used in this study [12]. Figure 3 shows the circuit model of Selenium IPMC.

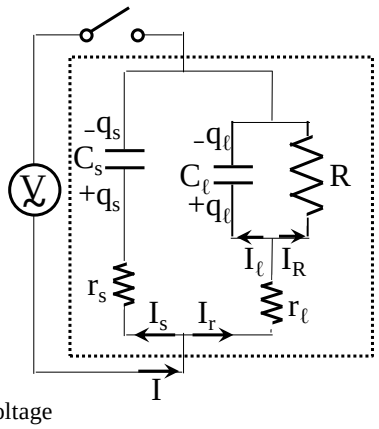

V: voltage
I : current
C: capacitance
r and R: resistance (r_ℓ: silver layer; R: Selemion CMV layer)

Fig 3: Circuit model Circuit encircled by dotted line represents the Selenium IPMC. The parameters used are described in ref. [12].

This circuit model suffices the following three conditions.

a. The total charge passing through r_ℓ (r_ℓ: sum of resistance of top and bottom silver layers) represented by $Q_r(t)$ and the charge stored in the capacitor C_ℓ represented by $Q_\ell(t)$ contribute to the bending induction, but the degree of induced bending curvatures by the unit charge of $Q_r(t)$ and $Q_\ell(t)$ are different.
b. The charge other than $Q_r(t)$ or $Q_\ell(t)$ did not cause any bending at all.
c. The bending curvature, B, of Selenium IPMC is given by Eq. (1), where the coefficient k_F and k_{nF} were determined experimentally as described in the ref. [12].

$$B = k_F Q_r(t) + k_{nF} Q_\ell(t) \quad (1)$$

It needs to obtain the formula of current for the circuit model in order to predict the bending curvature of Selenium IPMC. Using the current formula, $Q_r(t)$ and $Q_\ell(t)$ are computationally estimated, and substituted into Eq. (1) above. As described in ref. [12], the expression of the output current as a result of the first pulse (1st stage) is given by Eq. (2).

$$I(t) = \frac{q_s}{\tau_s}\exp\left(-\frac{t}{\tau_s}\right) + \frac{RC_\ell - \tau_\ell}{\tau_\ell RC_\ell} q_\ell \exp\left(-\frac{t}{\tau_\ell}\right) + \frac{q_\ell}{RC_\ell} \quad (2)$$

where $\tau_s = r_s C_s$, $q_s = C_s V$, $\tau_\ell = \frac{C_\ell r_\ell R}{r_\ell + R}$ and $q_\ell = \frac{R}{r_\ell + R} C_\ell V$.

q_s^T and q_ℓ^T respectively given by Eqs. (3.1) and (3.2) are used in deriving the formula of the output current resulting from the second pulse (2nd stage).

$$q_s^T \equiv q_s[1-\exp(-T/\tau_s)] \quad (3.1)$$

$$q_\ell^T \equiv q_\ell[1-\exp(-T/\tau_\ell)] \quad (3.2)$$

where T = 15 s.

2nd stage begins at t = T ≡ 15 s. The moment t = T is redefined as t' = 0 s now, and Eq. (4) representing the current at 2nd stage is derived.

$$I(t') = \frac{q_s - q_s^T}{\tau_s}\exp\left(-\frac{t'}{\tau_s}\right) + \frac{(q_\ell^T - q_\ell)(\tau_\ell - RC_\ell)}{RC_\ell \tau_\ell}\exp\left(-\frac{t'}{\tau_\ell}\right) + \frac{q_\ell}{RC_\ell} \quad (4)$$

The above equation contains a number of parameters (τ_s, τ_ℓ, q_s, q_ℓ, C_s, C_ℓ, r_s, r_ℓ, R), and the procedure of estimating those parameters are described in our previous paper, ref. [12]. In the ref. [12], all the parameters and kn and knF employed in Eq. (1) are assumed to be constant throughout the experiment. However, we found that the circuit model is not very accurate in predicting long term bending behavior of Selenium IPMC, as long as they were assumed to be constant. Hence, we assumed that all the parameters except for k_n and k_{nF} are discretely variable. Such a treatment to the circuit model is not so uncommon. In fact, some models take into consideration the change of IPMC characteristics in accordance with the experimental conditions [17,21]. The parameters except for k_F and k_{nF} are constant unless the stage changed, but once the voltage impose proceeded to next stage (definition of stage is given in Fig. 1), the parameters changes. Those parameters after the 2nd stage were estimated simply by extending the parameter estimation process shown in the ref. [12]. Figure 4 shows the transition history of estimated typical parameters, R, C_ℓ and r_ℓ.

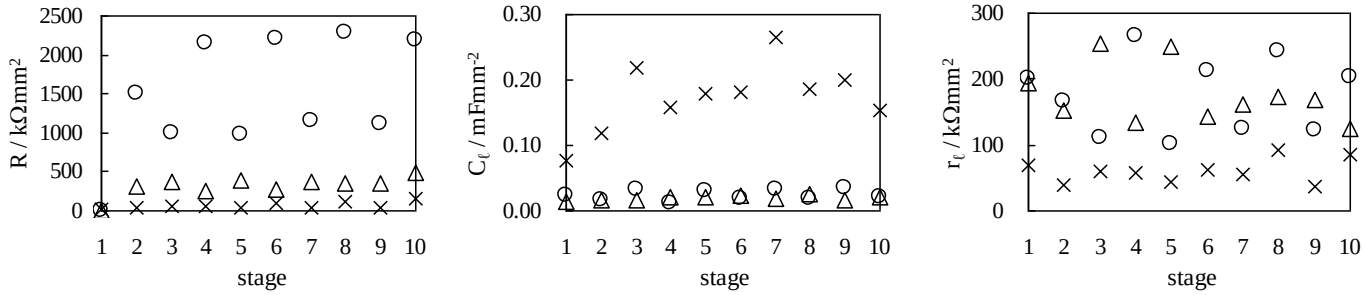

Fig 4: Transition behavior of typical parameters, R, C_ℓ and r_ℓ ○: AH = 4.5 gm^{-3} △: AH = 6.8 gm^{-3} ×: AH = 10.1 gm^{-3}

R represents the resistance of Selenium CMV layer of the Selenium IPMC. In the lowest absolute humidity environment, R takes quite large quantity at all the stage. It is quite natural result: A highly dehydrated Selenium IPMC is as intuitively understood prone to absorb water from its environment, and the water absorbed promoted the ionization of Selenium layer of the Selenium IPMC [14]. Ionization of Selenium IPMC improves the electrical conductivity of the Selenium layer. However, Selenium IPMC could not absorb enough quantity of water in the lowest absolute humidity environment. Thus, the resistance in Selenium layer in the low absolute humidity environment is quite high compared to a higher absolute humidity environment. On

the other hand, C_ℓ is quite large quantity for all the stages in the high absolute humidity environment. Due to the increase in the ionization level of Selenium layer in the high absolute humidity environment, a large quantity of ions are created within the Selenium CMV layer, resulting in the high capacitance. $r\ell$ does not exhibit so heavy dependence on the environmental absolute humidity unlike R and C_ℓ. r_ℓ represents the resistance of silver metal layers of Selenium IPMC. Ideally, the resistance of metal does not change and therefore r_ℓ is fairly constant. Thus it is concluded that the estimated parameters, R, C_ℓ, and r_ℓ, are quite accurate. The parameters other than R, C_ℓ, and r_ℓ (the data of which are not shown in this paper) were also quantitatively assessed and all of them were within the plausible range.

Using the above parameters and the circuit equation (Equation 4), the expression of $I_r(t)$, $I_\ell(t)$ and $I_R(t)$ for the 1st stage are given by Eqs. (5.1), (5.2) and (5.3), respectively. Eq. (6) is obtained using Eqns. (5.2) and (5.3).

$$I_s(t) = (q_s/\tau_s)\cdot\exp(-t/\tau_s) \quad (5.1)$$

$$I_\ell(t) = (q_\ell/\tau_\ell)\cdot\exp(-t/\tau_\ell) \quad (5.2)$$

$$I_R(t) = (q_\ell/RC_\ell)\cdot[1-\exp(-t/\tau_\ell)] \quad (5.3)$$

$$I_r(t) = I_\ell(t) + I_R(t) \quad (6)$$

By the time integration of $I_r(t)$ and $I_\ell(t)$, $Q_r(t)$ and $Q_\ell(t)$ are obtained. Plugging the numerical values of $Q_r(t)$ and $Q_\ell(t)$ into Eq. (1), the bending curvature of Selenium IPMC at the 1st stage can be computed. Bending curvature of further stages can be obtained basically in the same manner. Figure 2 shows the experimentally obtained relationship of curvature vs. charge of Selenium IPMC, and Figure 5 shows the computational result of curvature vs. charge obtained employing the circuit model. The computed result quite well reproduces the experimental result, and especially it is evident that the clockwise and counterclockwise rotational trajectories were well reproduced. The clockwise and counterclockwise trajectories are further analyzed next.

For AH < 10 gm^{-3}: The clockwise trajectory at AH < 10 gm^{-3} is analyzed using the experimental and computational results for AH = 4.5 gm^{-3} (AH < 10 gm^{-3}). It's worthy to note that the assumptions described earlier that only $Q_r(t)$ which is the charge passing through r_ℓ and another charge $Q_\ell(t)$ which is stored in C_ℓ contribute the induction of Selenium IPMC bending.

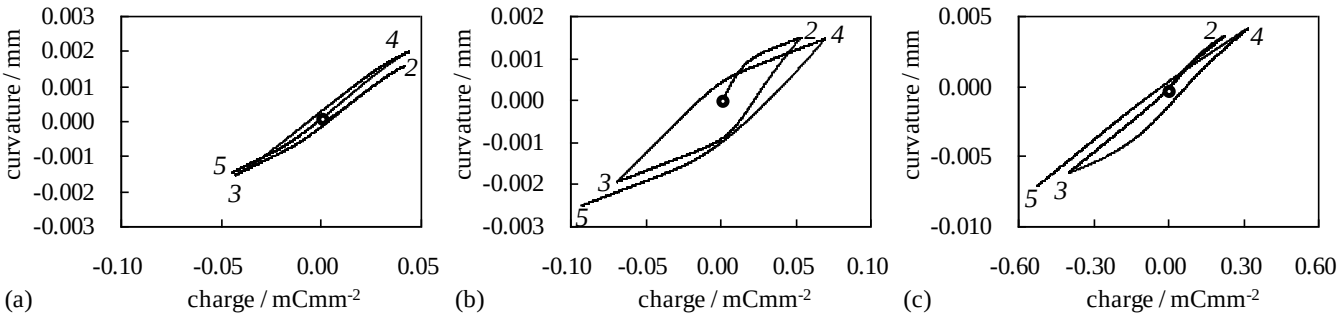

Fig 5: Computational results of curvature of Selenium IPMC vs. charge imposed on the unit surface area of Selenium IPMC at (a) AH = 4.5 gm^{-3}, (b) AH = 6.8 gm^{-3} and (c) AH = 10.1 gm^{-3} "O" mark in the diagram represents " t = 0 s ". Italic number represents the onset moment of individual stage, where the definition of stage is given in Fig. 1.

Figure 6 (a) shows the flow of charge at the 1st pulse: Once 1.5 V was imposed on the Selenium IPMC for 15 s at 1st pulse, total charge passing through the Selenium IPMC represented by $Q_{tot}(t)$ splits into two charges $Q_s(t)$ and $Q_r(t)$ as illustrated in Fig. 6 (a). Figure 7 (a) shows the computational result of time dependence of $Q_{tot}(t)$ and $Q_s(t)$ in case AH = 4.5 gm^{-3}. According to Fig. 7 (a), $Q_s(t)$ is negligibly small compared with $Q_{tot}(t)$. Hence, virtually whole charge of $Q_{tot}(t)$ passes through r_ℓ and a certain part of it is stored in C_ℓ, which was earlier denoted by $Q_\ell(t)$. Therefore, the bending of Selenium IPMC right after the onset moment of 1st stage is caused by both $Q_r(t)$ (~ $Q_{tot}(t)$) and $Q_\ell(t)$. Hence, the curvature represented by B rises rapidly as illustrated in Fig. 6 (a-1). Once the C_ℓ comes to be full of charge, only $Q_r(t)$ contributes to the bending induction, resulting in the low rate of curvature change as illustrated in Fig. 6 (a-2). At the 2nd stage, the voltage polarity is reversed as illustrated in Fig. 6 (b), and thus, the opposite process to the 1st stage is induced. Initially, both charges, $Q_r(t)$ and $Q_\ell(t)$, contribute to the bending induction. Hence, the magnitude of curvature rate is high as illustrated in Fig. 6 (b-1). However, as the C_ℓ comes to be full of charge, its contribution to the bending induction ceases. Therefore, only $Q_r(t)$ contributes to the bending induction. The magnitude of curvature rate decreases as illustrated in Fig. 6 (b-2). Every time the voltage polarity reversed, the same process proceeds. Therefore, the clockwise rotational diagram of curvature vs. charge is generated at AH < 10 gm^{-3}.

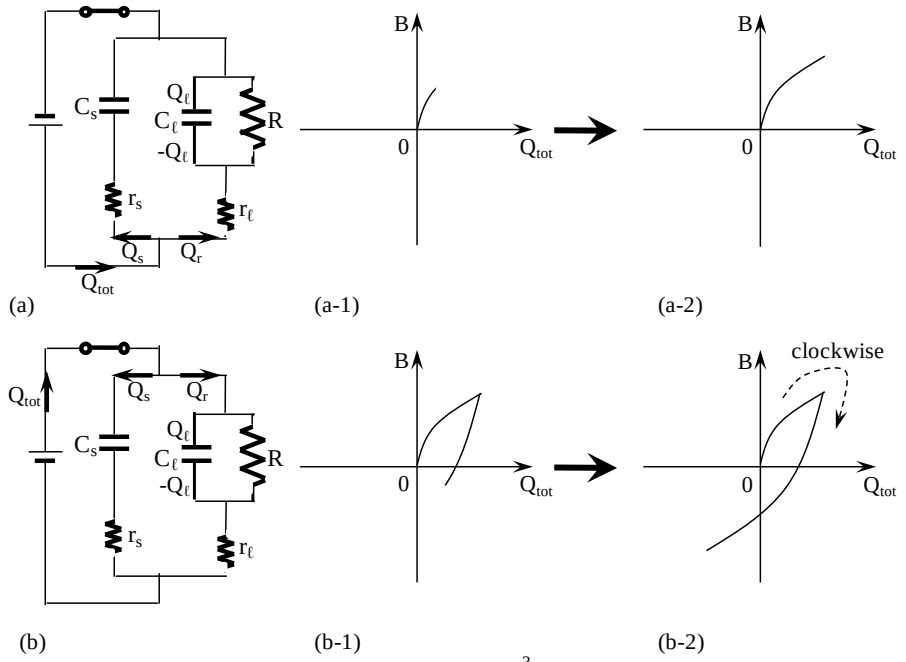

Fig 6: The output current polarity and B vs. Q_{tot} when AH < 10 gm^{-3} (a) circuit model for 1st stage (a-1) B vs. Q_{tot} with C_ℓ capacitance being low (a-2) B vs. Q_{tot} with C_ℓ capacitance being high (b) circuit model for 2nd stage (b-1) B vs. Q_{tot} with C_ℓ capacitance being low (b-2) B vs. Q_{tot} with C_ℓ capacitance being high

For AH > 10 gm^{-3}: Figure 7 (b) shows the computational result of Q_{tot} and Q_s for the Selenium IPMC under a pulsated voltage shown in Fig. 1 in the environment of absolute humidity of AH = 10.1 gm^{-3}. Prior to showing the explanation of bending behavior, the authors of this paper would like to urge readers to bear in mind that Q_s accounts for the large part of whole charge of Q_{tot} after the 2nd stage as clearly seen in Fig. 7 (b), although Q_s never induces bending of CMV IPMC by the assumption (II) which is described earlier in this section.

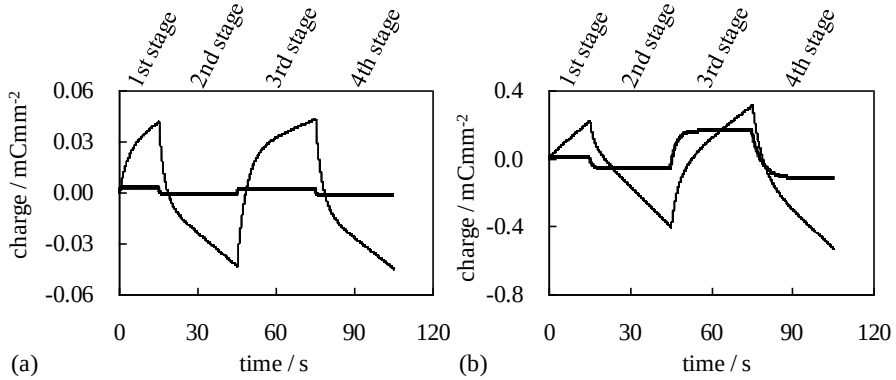

Fig 7: Fine line: Computational result of Q_{tot} vs. time Thick line: Computational result of Q_s vs. time (a) AH = 4.5 gm^{-3} (b) AH = 10.1 gm^{-3}

On the 1st stage, the current passing through r_s and C_s is negligibly small as indicated in Fig. 7 (b), which is similar phenomenon observed at the 1st stage shown in Fig. 7 (a). Thus a similar bending behavior to Fig. 6 (a-1) and (a-2) results as illustrated in Fig. 8 (a-1). After the 1st stage, the charge passing through r_s and C_s gradually becomes non-negligibly large as clearly seen in Fig. 7 (b). Voltage polarity is reversed at the beginning of 2nd stage. The ratio of Q_s (Note: Q_s does not contribute to the bending induction at all.) to Q_{tot} increases slightly over that in the 1st stage. Therefore, the magnitude of curvature rate at the 2nd stage is not as large as the curvature rate induced right after t = 0 s as illustrated in Fig. 8 (b-1). On the 3rd stage, a large current flows through r_s and is stored as charge Q_s in C_s for a while after the voltage polarity change at t = 45 s as shown in Fig. 7 (b). Therefore, the curvature does not change so significantly, though Q_{tot} clearly exhibits the increases. Hence, the trajectory takes the form shown in Fig. 8 (c-1). Gradually Q_s rises with current, and eventually the current flowing through r_s and C_s ceases. Hence, the total current flows through r_ℓ, and Q_ℓ increases, resulting in the increase of curvature rate as shown in Fig. 8 (c-2). The same process after the 3rd stage proceeds every time the voltage polarity reversed, resulting

in the transition from clockwise to counterclockwise rotation. As described at the end of Introduction, the bending behavior of Selenium IPMC is analyzed in the next section using the viscoelastic model. Computational procedure for obtaining the diagram of Selenium IPMC bending curvature vs. time is basically same as that described in the ref. [12].

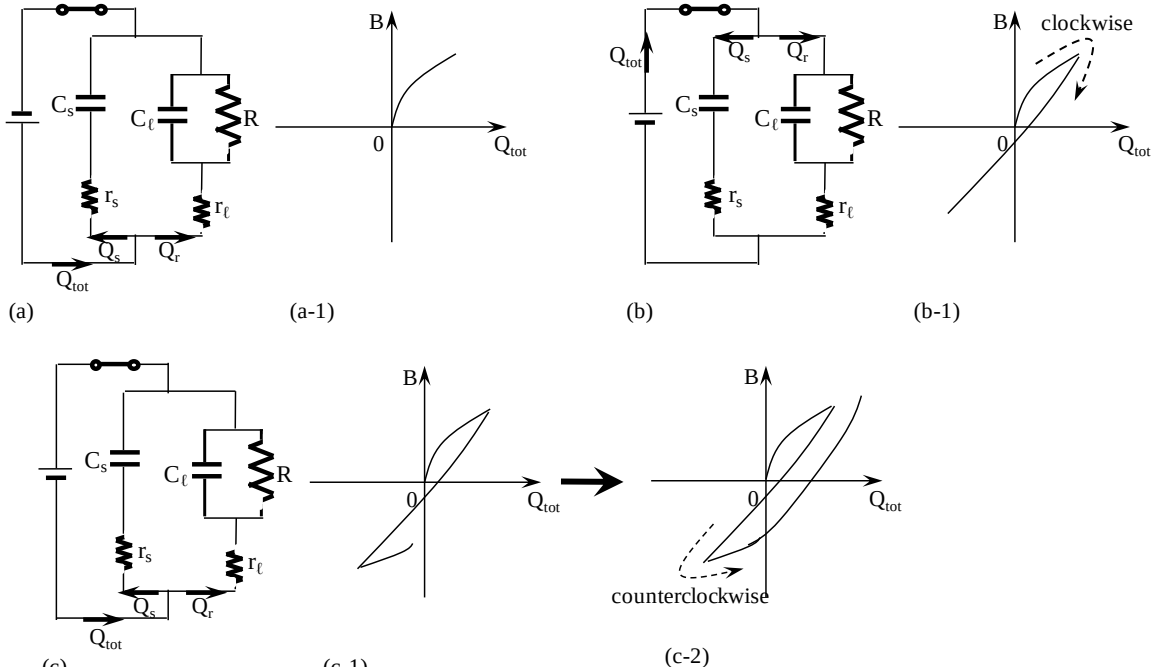

Fig 8: Circuit model and C vs. Q_{tot} when absolute humidity is high (a) circuit model for 1st stage (a-1) C vs. Q_{tot} (b) circuit model for 2nd stage (b-1) C vs. Q_{tot} (c) circuit model for 3rd stage (c-1) C vs. Q_{tot} before C_s being filled up with charge (c-2) C vs. Q_{tot} after C_s being filled up with charge**.** The input current polarity and B vs. Q_{tot} when absolute humidity is high (a) circuit model for 1st stage (a-1) B vs. Q_{tot} (b) circuit model for 2nd stage (b-1) B vs. Q_{tot} (c) circuit model for 3rd stage (c-1) B vs. Q_{tot} before C_s being filled up with charge (c-2) B vs. Q_{tot} after C_s being filled up with charge

4.3 Viscoelastic Model Analyses

As clearly seen in Fig. 2, the data curve of curvature vs. charge, which was obtained experimentally at AH > 10 gm^{-3}, exhibits the transition of rotational direction from clockwise to counterclockwise, while such a rotational direction transition does not happen at AH < 10 gm^{-3}. In this section, we attempt to reproduce the clockwise and counterclockwise trajectories by the use of viscoelastic model analysis introduced previously [23]. Concerning the clockwise rotation, previously we already succeeded in computationally reproducing the clockwise rotational data curve of curvature vs. charge [12], and that computational result is again introduced as Fig. 9 (a) in this paper.

The clockwise rotational data curve is clearly seen in it.The theoretical model employed for obtaining the diagram in Fig. 9 (a) was based on the viscoelastic model originally proposed in the ref. [23]. It was previously reported that that this viscoelastic model was reduced to the ordinary elastic model, resulting in Fig. 9 (a).[12] We again follow basically the same computational procedure employed in the ref. [12]. So, the theory used for the purpose of reproducing the counterclockwise rotational curve of curvature vs. charge was virtually the ordinary elastic model but originally the viscoelastic model.

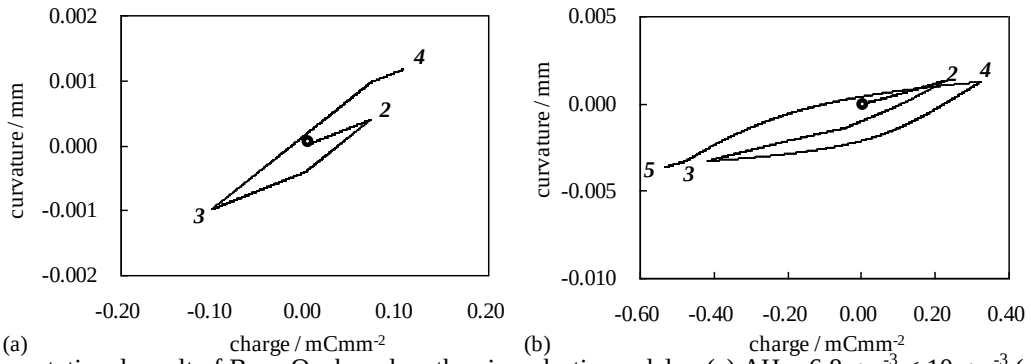

Fig 9: Computational result of B vs. Q_{tot} based on the viscoelastic model (a) AH = 6.8 gm^{-3} < 10 gm^{-3} (same as Fig 21 (a) of the ref. [12]) (b) AH = 10.1 gm^{-3} > 10 gm^{-3}. "O" mark in the diagram represents "t = 0 s". Italic number represents the onset moment of individual stage, where the definition of stage is given in Fig. 1.

The transition from clockwise to counterclockwise direction (Fig. 2 (c)), cannot be computationally reproduced merely by following the same computational procedure as previously introduced.[12] It is necessary to modify the way of analysis. We will explain the procedure of computationally reproducing the data curve of Fig. 2 (b).

Eq. (7.1) represents the Selenium IPMC in the free bending state with the boundary and the initial conditions as indicated by Eq. (7.2) [12], where y(t, x) is the vertical position of the Selenium IPMC beam at given position x at time t (definition of coordinate is illustrated in Fig. 10), l represents the length between the origin (x, y) = (0, 0) and the free end of Selenium IPMC (see Fig. 10), and the dot and the prime represent the differentiation with respect to t and x, respectively.

In Eq. (7.1), E_{fb} (t)) is the time-dependent Young's modulus of the Selenium IPMC in the free bending state, I_m is the moment of inertia of the cross section of the beam, and f(t) is the force per unit width (1 mm) of the Selenium IPMC (see Fig. 10).

$$\int_0^t E_{fb}(t - \square)\cdot I_m \cdot \dddot{y}(\square, x)\, d\square + f(x) = 0 \qquad (7.1)$$

$$y(t,0) = 0,\ y'(t,0) = 0,\ y''(t,l) = 0,\ y(0,x) = 0 \qquad (7.2)$$

The applied voltage is low and thus the Selenium IPMC does not exhibit a large deformation, which implies that the bending curvature is obtained by y''(t, x). In solving Eq. (7.1) with respect to y(t, x), $E_{fb}(t)$ should be known. It was shown in the ref. [12] by theoretical calculation that the Young's modulus of Selenium IPMC is almost constant with respect to time under the applied voltage. $E_{fb}(t)$ was estimated to be $E_{fb}(t) = E_0 = 2.54$ GPa, and this value was employed in this work. Solving Eq. (7.1) with respect to x under the conditions Eq. (7.2) and $E_{fb}(t) = 2.54$ GPa, the vertical displacement y(t, x) of Selenium IPMC at given point x at time t is given as

$$y(t,0) = [f(t)/2I_m \cdot E_o]\cdot(lx^2 - x^3/3) \qquad (8)$$

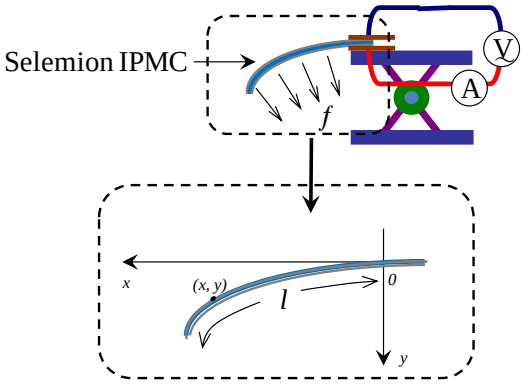

Fig 10: Coordinate system set to the Selenium IPMC in the process of free bending, where the Selenium IPMC is clamped between a pair of electrodes at the origin of coordinate system. Coordinate (x, y) is a representative point of Selenium IPMC top surface. f is the force exerted on the Selenium IPMC from its inside, causing the Selenium IPMC bending, when the Selenium IPMC is under voltage. l is the length of Selenium IPMC from the origin to its free end.

According to the ref. [24], the blocking force by a Selenium IPMC (The IPMC used in the ref. [24] is called CMV IPMC, and it is same as Selenium IPMC) is proportional to the charge imposed on it, and f is the proportional to the blocking force. Therefore, f is considered to be proportional to the charge imposed on the Selenium IPMC as given by Eq. (9).

$$f = K\cdot[q_1(t) - q_2(t)] \qquad (9)$$

Here, we have to comment on f. Though it is described that f is same as the blocking force according to the basic concept of strength of materials [12], it is wrong. f is proportional to the blocking force according to the basic concept of strength of materials. However, the rest of the discussion described in the ref. [12] does not need to be altered at all. The value of constant K was previously estimated by an experiment described in the

ref [12] as K = 0.639, and this is the value used in this work. Hence, only $q_1(t)$ and $q_2(t)$ are the unknown values of f. If we can obtain $q_1(t)$ and $q_2(t)$ at a given time t = t', we can obtain f at t = t' using Eq. (9). Therefore, y(t = t', x) can be obtained by Eq. (8). $q_1(t)$ and $q_2(t)$ are evaluated by the following procedure: To derive q_1 and q_2, when the Selenium IPMC under a rectangular voltage pulse train, firstly the explicit formulas of the charge as a function of time are in need. Based on the circuit model shown earlier, it is assumed that the current takes the forms represented by

$$I_1(t) = I_{10} + I_{11}e^{-\beta_{11}t} + I_{12}e^{-\beta_{12}t} \qquad 0\text{ s} < t < 15\text{ s}$$

$$I_2(t) = I_{20} + I_{21}e^{-\beta_{21}(t-15)} + I_{22}e^{-\beta_{22}(t-15)} \qquad 15\text{ s} < t < 45\text{ s} \qquad (10)$$

$$I_3(t) = I_{30} + I_{31}e^{-\beta_{31}(t-45)} + I_{32}e^{-\beta_{32}(t-45)} \qquad 45\text{ s} < t < 75\text{ s}$$

$$I_4(t) = I_{40} + I_{41}e^{-\beta_{41}(t-75)} + I_{42}e^{-\beta_{42}(t-75)} \qquad 75\text{ s} < t < 105\text{ s}$$

i = 1, 2, 3, 4; j = 0, 1, 2; k = 1, 2 for I_i, I_{ij} and β_{ik}.

Hence, the formulas of charge are given as simple expressions as below. Since the charge changes continuously, $Q_2(15)$, $Q_3(45)$ and $Q_4(75)$ are same as

$Q_1(15)$, $Q_2(45)$ and $Q_3(75)$, respectively.

$$Q_1(t) = I_{10}t + I_{11}/\beta_{11}(1 - e^{-\beta_{11}t}) + I_{12}/\beta_{12}(1 - e^{-\beta_{12}t}) \qquad 0\text{ s} < t < 15\text{ s}$$

$$Q_2(t) = Q_1(15) + I_{20}(t-15) + I_{21}/\beta_{21}(1 - e^{-\beta_{21}(t-15)}) + I_{22}/\beta_{22}(1 - e^{-\beta_{22}(t-15)}) \qquad 15\text{ s} < t < 45\text{ s} \qquad (11)$$

$$Q_3(t) = Q_2(45) + I_{30}(t-45) + I_{31}/\beta_{31}(1 - e^{-\beta_{31}(t-45)}) + I_{32}/\beta_{32}(1 - e^{-\beta_{32}(t-45)}) \qquad 45\text{ s} < t < 75\text{ s}$$

$$Q_4(t) = Q_3(75) + I_{40}(t-75) + I_{41}/\beta_{41}(1 - e^{-\beta_{41}(t-75)}) + I_{42}/\beta_{42}(1 - e^{-\beta_{42}(t-75)}) \qquad 75\text{ s} < t < 105\text{ s}$$

i = 1, 2, 3, 4; j = 0, 1, 2; k = 1, 2 for I_i, I_{ij} and β_{ik}.

The parameters in Eq. (10) are required in order to quantitatively evaluate Eq. (11). Using the experimental data of current in conjunction with the data shown in Fig. 2 (c) at AH = 10.1 gm^{-3}, those parameters were estimated employing by the curve fitting technique The technique used was the Newton method as described below.

$I_{10} = 0.0135$, $I_{11} = 0.0285$, $I_{12} = 0.00457$,
$\beta_{11} = 4.34$, $\beta_{12} = 0.215$
$I_{20} = -0.0137$, $I_{21} = -0.0858$, $I_{22} = -0.00918$,

$\beta_{21} = 0.95$, $\beta_{22} = 0.0464$ (12)

$I_{30} = 0.0116$, $I_{31} = 0.0297$, $I_{32} = 0.0921$,
$\beta_{31} = 36.5$, $\beta_{32} = 0.233$

$I_{40} = -0.0134$, $I_{41} = -0.0341$, $I_{42} = -0.0788$,
$\beta_{41} = 21.6$, $\beta_{42} = 0.172$

The current is positive from t = 0 s to 15 s and from 45 s to 75 s, while it is negative from t = 15 s to 45 s and from t = 75 s to 105 s. From Eq. (12), Eq. (13) was obtained.

$$Q_1(t) = 0.0278 + 0.0135t - 0.00657e^{-4.34t} - 0.0212e^{-0.215t}$$

$$Q_2(t) = -0.0584 - 0.0137(t-15) + 0.0903e^{-0.95(t-15)} + 0.198e^{-0.0464(t-15)} \qquad (13)$$

$$Q_3(t) = -0.0241 + 0.0116(t-45) - 0.000815e^{-36.5(t-45)} - 0.395e^{-0.233(t-45)}$$

$$Q_4(t) = -0.137 - 0.0134(t-75) + 0.00158e^{-21.6(t-75)} + 0.459e^{-0.172(t-75)}$$

In ref. [12], we define q_1 and q_2 in each stage by using $Q_i(t)$ (i = 1, 2, 3, 4) as is, since we investigated the Selenium IPMC bending behavior at AH < 10 gm^{-3}. For example, we can set $q_1 = Q_1(t)$ and $q_2 = 0$ $mC \cdot mm^{-2}$ in the 1st stage. However, such a procedure is inappropriate, as long as the environmental absolute humidity is greater than 10 gm^{-3}. According to the circuit model, the charge passing through the Selenium IPMC is responsible for the bending induction. However, not the whole current is responsible for the bending induction, and Q_s has nothing to do with the bending induction, where the definition on Q_s is given in Figs. 6 and 8. In case AH < 10 gm^{-3}, $|Q_s|$ is negligibly small compared to $|Q_{tot}|$, where the definition on Q_{tot} is given in Fig. 6 and 8. Hence, it is not necessary to pay much attention to Q_s behavior for quantitatively evaluating the bending curvature of Selenium IPMC. On the other hand, in case AH > 10 gm^{-3}, $|Q_s|$ is not negligibly small at all compared to $|Q_{tot}|$ (see Fig. 7 (b)), and Qs does not cause the bending of Selenium IPMC as described already. Therefore, we have to delete the exponentially decaying term with a smaller exponent β_{i2} from $I_i(t)$ (i = 1, 2, 3, 4) for the purpose of quantitatively and precisely evaluating the bending curvature of CMV IPMC. Here we denote the effective charges involved in the CMV bending induction by $Q_i^e(t)$ (i = 1, 2, 3, 4). They are explicitly represented by

$$Q_1^e(t) = 0.00657 + 0.0135t - 0.00657e^{-4.34t}$$

$$Q_2^e(t) = -0.0903 - 0.0137(t-15) + 0.0903e^{-0.95(t-15)} \qquad (14)$$

$$Q_3^e(t) = 0.000815 + 0.0116(t-45) - 0.000815e^{-36.5(t-45)}$$

$$Q_4^e(t) = -0.00158 - 0.0134(t-75) + 0.00158e^{-21.6(t-75)}$$

Note that $Q_1^e(0)$, $Q_2^e(15)$, $Q_3^e(45)$ and $Q_4^e(75)$ are 0.

Based on the discussion above and the argument in ref. [12], we took the following procedure for computing q_1 and q_2 in each stage in case the absolute humidity is high. We firstly set $q_1 = Q_1^e(t)$ and $q_2 = 0$ from t = 0 s to 15 s. After the polarity of the applied voltage is reversed, $q_1 = Q_1^e(15) + Q_2^e(t)$ and $q_2 = -Q_2^e(t)$ until q_1 becomes 0. Since q_1 is equal to 0 at t = 23.7 s from the definition of Eq. (14), $q_1 = 0$ and $q_2 = Q_1^e(15)$ at t = 23.7 s. Then, we set $q_1 = 0$ and $q_2 = -Q_2^e(t)$ from t = 23.7 s to 45 s. By the same argument, $q_1 = Q_3^e(t)$ and $q_2 = Q_2^e(45) - Q_3^e(t)$ from 45 s to 75 s. Note that $Q_2^e(45) - Q_3^e(t)$ decreases in time but does not attain 0 from 45 s to 75 s. So, we set $q_1 = Q_3^e(75) + Q_4^e(t)$ and $q_2 = Q_2^e(45) - Q_3^e(75) - Q_4^e(t)$ from 75 s to 100.9 s, and $q_1 = 0$ and $q_2 = Q_2^e(45) - Q_3^e(75) - Q_4^e(t)$ from 100.9 s to 105 s. Note that $q_1 = 0$ at t = 100.9 s.

Fig. 9 (b) shows the computational result of Selenium IPMC bending curvature vs. time using the viscoelastic model in case AH = 10.1 gm-3 (Bear in mind that the horizontal axis of Fig. 9 is not the effective charge given by Eq. (14) but the total charge of Q_{tot} which includes Q_s.) Quite intriguingly, the transition of clockwise rotation – the 1st stage → 2nd stage → 3rd stage – to counterclockwise rotation – the 2nd stage → 3rd stage → 4th stage - is computationally achieved. It is a typical characteristics of Selenium IPMC experimentally observed at AH > 10 gm^{-3}, where the experimental data is shown in Fig. 2 (c), although the initial clockwise rotation – the 1st stage → 2nd stage → 3rd stage – is not so clearly induced. To sum up, not only the circuit model but even the viscoelastic model reproduces the unusual a bit complex behavior of Selenium IPMC. The rotational direction change is explicable in terms of charge flow behavior by appropriately evaluating and treating the charge.

So far, we have not found out a reason of the increase of the magnitude of Q_s/Q_{tot} with the increase of absolute humidity. It is an issue of physical chemistry of IPMC. Still we need to continue to study the IPMC characteristics.

5. CONCLUSION

A number of researchers have attempted to fabricate an electrically-bending-controllable IPMC-based actuator for the past decades by scrutinizing the characteristics of IPMC. Although the IPMC studied by those researchers are different from the Selenium IPMC, our research results indicate that even the slight environmental absolute humidity change causes large alteration of bending behavior of IPMC. Such complex bending behavior was due to the mutually distinctive influence of individual charges, which flows through or stored in the Selenium IPMC, on the bending induction and also due to the discrete change of IPMC characteristics in accordance with the experimental condition of the environmental absolute humidity and the polarity of voltage imposed on the IPMC. It is interpreted as the IPMC's electromechanical characteristics are not so easily explicable or controllable. For achieving a practical IPMC actuator it needs to investigate the IPMC characteristics by far deeply than we have thought.

ACKNOWLEDGMENT

This research was conducted under the financial support of the Ministry of Education, Science, Sports and Culture, Grant-in-Aid for Challenging Exploratory Research, 26650032, 2014.

REFERENCES

[1] K. Oguro, Y. Kawami, H. Takenaka, "Bending of an ion-conducting polymer film–electrode composite by an electric stimulus at low voltage", Trans. J. Micromach. Soc., 1992, 5, pp.27–30.

[2] K. Oguro, K. Asaka, H. Takenaka, "Polymer film actuator driven by low voltage", Proc. 4th International Symposium on Micro Machine and Human Science, Nagoya, Japan, 1993, pp.39–40.

[3] K. Asaka, K. Oguro, Y. Nishimura, M. Mizuhara, H. Takenaka, "Bending of polyelectrolyte membrane–platinum composite by electric stimuli I, response characteristics to various waver forms", Polym. J., 1995, 27, pp.436–440.

[4] K. Salehpoor, M. Shahinpoor, M. Mojarrad, "Linear and platform type robotic actuators made from ion-exchange membrane–metal composites", Proc. SPIE Smart Mater. Struct., San Diego, CA, 1997, 3040, pp. 192–198.

[5] M. Shahinpoor, Y. Bar-Cohen, T. Xue, J. O. Simpson, J. Smith, "Some Experimental Results on Ionic Polymer-Metal Composites (IPMC) As Biomimetic Sensors and Actuators", Proc. SPIE Smart Mater. Struct., 1998, 3324, pp. 251–267.

[6] Y. Bar-Cohen, T. Xue, M. Shahinpoor, K. Salehpoor, J. Simpson, J. Smith, "Low mass muscle actuators using electroactive polymers (EAP)", Proc. SPIE Smart Mater. Struct., 1998; San Diego, CA, Paper-No. 324–32, 1998.

[7] M. Uchida, M. Taya, "Solid polymer electrolyte actuator using electrode reaction", Polymer, 2001, 42, pp.9281–9285.

[8] S. Nemat-Nasser, "Micromechanics of Actuation of Ionic Polymer-metal Composites", J. App. Phys., 2002. 92, pp. 2899–2915.

[9] S. Nemat-Nasser, Y. Wu, "Comparative Experimental Study of Ionic Polymer-Metal Composites with Different Backbone Ionomers and in Various Cation Forms", J. App. Phys., 2003, 93, pp.5255–5267.

[10] Y. Wang, H. Chen, Y Wang, Z. Zhu, D. Li, "Effect of Dehydration on the Mechanical and Physicochemical Properties of Gold- and Palladium-Ionomeric Polymer-Metal Composite

(IPMC) Actuators", Electrochimica Acta, 2014, 129, pp.450–458.

[11] R. K. Jain, S. Datta, S. Majumder, "Design and control of an IPMC artificial muscle finger for micro gripper using EMG signal", Mechatronics, 2013, 23, pp.381–394.

[12] K. Ikeda, M. Sasaki, H. Tamagawa, "IPMC bending predicted by the circuit and viscoelastic models considering individual influence of Faradaic and non-Faradaic currents on the bending", Sensors and Actuators B: Chemical, 2014, 190, pp.954–967.

[13] H. Tamagawa, F. Nogata, "Bending response of dehydrated ion exchange polymer membrane to the applied voltage", J. Membrane Sci., 2004, 243, pp.229–234.

[14] H. Tamagawa, F. Nogata, M. Sasaki, "Charge quantity as a sole factor quantitatively governing curvature of Selemion", Sensors and Actuators B: Chemical, 2007, 124, pp.6-11.

[15] Y. Onouchi, M. Sasaki, H. Tamagawa, "Current-controlled Selemion bending in the controlled humidity environment", Sensors and Actuators B: Chemical, 2009, 135, pp.465-471.

[16] H. Tamagawa, F. Nogata, T. Watanabe, A. Abe, K. Yagasaki, J.-Y. Jin, "Influence of metal plating treatment on the electric response of Nafion", J. Mater. Sci. 2003, 38, pp.1039-1044.

[17] M. Porfiri "Charge dynamics in ionic polymer metal composites", J. Appl. Phys., 2008, 104, 104915.

[18] P. J. C. Branco, J. A. Dente, "Derivation of a continuum model and its electric equivalent-circuit representation for ionic polymer-metal composite (IPMC) electromechanics", Smart Materials and Structures, 2006, 15, pp.378-392.

[19] K. Farinholt, J. L. Donald, "Modeling of electromechanical charge sensing in ionic polymer transducers", Mechanics of Materials, 2004, 36, pp.421-433.

[20] X. Bao, Y. Bar-Cohen, S. Lih, "Measurements and macro models of nonnumeric polymer-metal composites (IPMC)", Proc. SPIE Smart Mater. Struct., San Diego, CA, 2002; 4695, pp.220–227.

[21] Z. Chen, D. R. Hedgepeth, X. Tan, "A Nonlinear Control-Oriented Model for Ionic Polymer-Metal Composite Actuators", Smart Materials and Structures, 2008, 18, pp.1-9.

[22] K. Park, B. Lee, H.-M. Kim, K.-S. Choi, G. Hwang, G.-S. Byun, H.-K. Lee, "IPMC Based Biosensor for the Detection of Biceps Brachii Muscle Movements", Int. J. Electrochem. Sci. 2013, 8 pp.4098-4109.

[23] K. Yagasaki, H. Tamagawa, "Experimental estimate of viscoelastic properties for ionic polymer-metal composites", Phys. Rev. E, 2004, 70, 052801-1-4.

[24] H. Tamagawa, F. Nogata, "Dominant factor for the precise bending control of Selemion", Sensors and Actuators B: Chemical, 2006, 120, pp.19–24.

AUTHOR PROFILE

K. Ikeda obtained PhD from Tohoku University, Japan in 2008. He is a lecturer in Meiji University, Japan and currently involved in the research on pattern formation problems and reaction diffusion equations.

M. Sasaki obtained PhD from Tohoku University, Japan in 1985. He is a professor in Gifu University, Japan and currently involved in the research on robotics and control theory.

H. Tamagawa obtained PhD from Tokyo Institute of Technology, Japan in1997. He is an assistant professor in Gifu University in Japan and currently involved in the research on the biomaterials, especially electroactive polymers.